CEA Comité Español de Automática

XLV JORNADAS AUTOMÁTICA MÁLAGA 2024

UNIVERSIDADE DA CORUÑA

Jornadas de Automática

Temperature control for a PEM electrolyser powered by a renewable source.

Barros-Queiroz, J. S.[a,b,*], Torrico, B. C.[a], Nogueira, F. G.[a], Bordons, C.[b], Ridao, M. A.[b]

[a] *Departamento de Engenharia Elétrica, Universidade Federal do Ceará (UFC), Fortaleza, CE, Brazil.*
[b] *Dpto. de Ingeniería de Sistemas y Automática, Universidad de Sevilla, Camino de los Descubrimientos s/n., 41092 Sevilla, Spain.*

To cite this article: Barros-Queiroz, J. S., Torrico, B. C., Nogueira, F.G., Bordons, C., Ridao, M. A. 2024. Temperature control for a PEM electrolyser powered by a renewable source.
Jornadas de Automática, 45. https://doi.org/10.17979/ja-cea.2024.45.10894

Resumen

Este artículo aborda el desarrollo y la aplicación de un controlador basado en modelo para un electrolizador PEM (Membrana de Intercambio de Protones). El objetivo principal es optimizar el control de temperatura, buscando una mayor eficiencia en la producción de hidrógeno y una vida útil más prolongada del sistema. Estos dos beneficios se ven comprometidos cuando el electrolizador se somete a altas temperaturas que superan su temperatura nominal. Esto puede ocurrir cuando el sistema es alimentado por fuentes renovables, ya que debido a la variabilidad e intermitencia de su generación, pueden operar con altas densidades de corriente eléctrica. El controlador propuesto emplea junto con el MPC (Control Predictivo Basado en Modelo) un modelo de perturbación para promover el desacoplamiento en el tratamiento de las perturbaciones e introducir un grado de libertad adicional en la estrategia de control. Los resultados de la simulación demuestran el rendimiento robusto del controlador en el manejo de las no linealidades del sistema, asegurando que la temperatura del electrolizador se mantenga en un nivel seguro para la preservación del sistema.

Palabras clave: Hidrógeno verde, Electrolizador PEM, Control predictivo basado en modelo, Modelo de Perturbación, Control de Temperatura.

Control de temperatura para un electrolizador PEM alimentado por una fuente renovable.

Abstract

This article addresses developing and applying a model-based controller for a PEM (Proton Exchange Membrane) electrolyser. The primary objective is to optimise temperature control, aiming for greater efficiency in hydrogen production and extended system lifespan. These two benefits are compromised when the electrolyser is subject to high temperatures exceeding its nominal temperature. Such conditions can occur when the system is powered by renewable sources, which can operate at high current densities due to their variability and intermittency. The proposed controller employs an MPC (Model Predictive Control) combined with a disturbance model to promote decoupling in handling disturbances and introduce an additional degree of freedom to the control strategy. Simulation results demonstrate the robust performance of the controller in managing system nonlinearities, ensuring that the electrolyser temperature remains at a safe level for system preservation.

Keywords: Green hydrogen, PEM electrolyser, Model Predictive Control, Disturbance model, Temperature Control.

1. Introduction

Energy transition is crucial for reducing greenhouse gas (GHG) emissions and ensuring a sustainable future. It involves shifting the energy matrix from fossil fuel-based sources like oil, natural gas, and coal to renewable sources like solar, wind, hydropower, and biomass. This transition is essential to achieve the emission reduction goals of the Paris Agreement (2015) (Maia and Garcia, 2023).

Another international agreement signed in 2015, the 2030

*Autor para correspondencia: julsobbar@alum.us.es
Attribution-NonCommercial-ShareAlike 4.0 International (CC BY-NC-SA 4.0)

Agenda for Sustainable Development, aims to achieve 17 Sustainable Development Goals (SDGs), including climate action (SDG 13), affordable and clean energy (SDG 7), and sustainable cities and communities (SDG 11) (United Nations, 2015). Similarly, many other agreements focus on sustainability and decarbonization, which are essential for environmental protection and transitioning to a low-carbon economy. This broader concept includes energy transition and a range of strategies and policies to reduce carbon emissions across all economic sectors.

Green hydrogen is a promising alternative for clean energy production and storage in the energy transition (Carmo et al., 2013). The most extended process to produce it is water electrolysis, which uses electricity to split water molecules (H_2O) into hydrogen (H_2) and oxygen (O_2). It is called green because the energy used for electrolysis comes from renewable sources. Electrolysers, which are the heart of the operation, convert electrical energy into chemical energy and produce pure hydrogen.

The advantages of green hydrogen are manifold, making it a compelling clean energy solution. It is a source of energy that leaves no carbon footprint, emitting no CO_2 during production or use, thereby contributing to a healthier environment. Its ability to be stored and transported for use during high-demand periods or when renewable sources are unavailable enhances its practicality. But perhaps its most significant advantage is its versatility. It can be used across diverse sectors, including transportation, industry, power generation, and residential heating, making it a promising solution for various energy needs. This versatility sets green hydrogen apart and makes it a key player in the energy transition.

As mentioned before, an electrolyser is a system that facilitates water electrolysis, a non-spontaneous redox chemical reaction that necessitates an external electric current. It comprises two inert electrodes separated by an electrolyte, which serves as the medium for ion movement between the anode and the cathode, enabling electrolysis. The electrolyte can exist in a liquid or solid state and can be classified into four types: alkaline water electrolysis (AWE), polymer electrolyte membrane (PEM), solid oxide electrolyte (SOE), and anion exchange membrane (AEM). The alkaline type, a more established and cost-effective technology, operates with low current densities. The PEM type is well-suited for use with renewable sources like wind and solar, because operating with high current densities and the dynamic is fast. However, they are manufactured with noble materials such as platinum, which makes their costs very high. The SOE type, still in the research and development phase, is used for high-temperature operations and is associated with a higher cost. AEM electrolysis is a promising technology that does not need noble materials and can run on pure water, although there are some open challenges as the durability of the membrane and the gases cross-over.

Benghanem et al. (2024) show that a PEM electrolyser powered by photovoltaic energy (PV-PEM) has greater efficiency than the PV-Alkaline system, and the total system efficiency decreases from 15 % to 8 % with the increase of incident solar irradiation. This fact occurs due to the amount of current density supported by each electrolyte.

Therefore, controlling the temperature of a PEM electrolyser would make its use more economically viable. Operating at temperatures close to its maximum operational limit results in higher hydrogen production, and ensuring this limit is not exceeded guarantees a longer lifespan, reducing damage to the membrane from high temperatures. In light of this, some authors have recently proposed temperature control strategies for this electrolyser.

Ogumerem and Pistikopoulos (2020) utilized an explicit Model Predictive Control (MPC), also known as eMPC, which was implemented in a laboratory-scale PEM electrolyser system. This controller was designed to maintain the water temperature differential across the stack within a safe range, aiming to preserve the membrane's integrity for longer. The control strategy was implemented on a microcontroller, thereby creating an embedded control system for continuous hydrogen production.

Keller et al. (2022) employ a model-based adaptive temperature control for a 100 kW PEM electrolyser. The control is implemented using a conventional Proportional-Integral-Derivative (PID) control approach to meet the dynamic requirements of the PEM electrolysis system. Additionally, a model-based feedforward control is utilized to effectively manage the stack temperature, ensuring it remains close to the desired setpoint, even in the face of dynamic disturbances in current density.

Molina et al. (2024) propose heat management in a PEM water electrolyser through a system composed of various elements, including PID control, water pumping circuit, air cooler, thermal insulation, and constant monitoring and adjustment. The PID control adjusts the air cooler speed based on two temperature transmitters, thus regulating the stack temperature and maintaining the desired temperature difference between the stack's inlet and outlet, contributing to the system's energy efficiency.

Therefore, given the critical role of temperature control in the performance and robustness of a PEM electrolyser, this work proposes a novel strategy based on model-based predictive control and a measured disturbance model. The strategy is designed to ensure optimal performance within the specified reference range, thereby enhancing control robustness.

The next sections are organised as follows. Section 2 presents the dynamic system and its linearization. Section 3 exposes the design of the proposed controller. Simulation results are shown in Section 4. Finally, concluding remarks are given in Section 5.

2. The dynamic system

To ensure proper operation, electrolysers are supported by auxiliary systems such as water purification, gas-liquid separators, hydrogen purification, power supply, sensors and control units, cooling systems, pumps, valves, piping, and more.

For example, when a continuous voltage is applied between the anode and cathode electrodes, the electrolysis process occurs within the electrolyser, producing H_2 at the cathode and O_2 at the anode, both containing a small amount of water. The resulting product then passes through gas-liquid separators, which remove the residual water mixed with the gases, ensuring that the hydrogen and oxygen produced are

as pure as possible. The water removed during the separation process is generally recirculated back into the electrolyser through the anode, enhancing system efficiency and reducing water waste.

Espinosa-Lopez et al. (2018) describe how the process of recirculating the water used in electrolysis works when coupled with a refrigeration system. In turn, the cooling system maintains the temperature within an ideal range, ensuring that the electrolyser operates efficiently and safely, prolonging its useful life and guaranteeing the quality of the products generated.

As previously mentioned, high temperatures pose a significant threat. They accelerate the degradation of the materials that make up the electrodes and the electrolyser membrane, cause overheating in the system, affect the electrical conductivity of its components, and influence the degree of purity of the gases produced.

The dynamic system was modeled by Mora and Bordons (2022), based on the system described by Espinosa-Lopez et al. (2018), using the phenomenological model of the electrolyser, which uses electrochemical equations to obtain the static characteristics and thermal equations to capture the system's dynamics.

The model is determined from the energy balance, using (1):

$$\frac{dT_{el}}{dt} = \frac{1}{C_t}(\dot{Q}_{gen} - \dot{Q}_{loss} - \dot{Q}_{cool}), \tag{1}$$

in which T_{el} is the electrolyser temperature (K), C_t is the thermal capacity of the stack (J/K), $\dot{Q}_{gen}$ is the heat generated in the system due to the irreversibilities or overvoltages of the process (W), $\dot{Q}_{loss}$ is the heat that is lost by interaction with the environment by convection and radiation (W), and $\dot{Q}_{cool}$ is the heat dissipated by the cooling system (W).

Thus,

$$\dot{Q}_{gen} = n_c I_{el}(V_{el} - V_{tn}), \tag{2}$$

and

$$\dot{Q}_{loss} = \frac{1}{R_t}(T_{el} - T_{amb}), \tag{3}$$

in which n_c is the number of cells, I_{el} is the current applied to the electrolyser, V_{el} is the voltage applied to the electrolyser from the electrochemical model, V_{tn} is the thermoneutral voltage, R_t is the thermal resistance, and T_{amb} is the ambient temperature.

Then, replacing (2) and (3) in (1):

$$\frac{dT_{el}}{dt} = \frac{1}{C_t}[n_c I_{el}(V_{el} - V_{tn}) - \frac{1}{R_t}(T_{el} - T_{amb}) - \dot{Q}_{cool}]. \tag{4}$$

Equation (4) represents a non-linear first-order differential equation that depends on the state/output and its derivatives (T_{el},$\dot{T}_{el}$), disturbances (I_{el},T_{amb}), and the input or control action ($\dot{Q}_{cool}$). The nonlinearity of this system is a consequence of the non-linear behavior of the two disturbances, I_{el} and T_{amb}. Consequently,

$$f(T_{el}, \dot{T}_{el}, I_{el}, T_{amb}, \dot{Q}_{cool}) = 0. \tag{5}$$

With the electrolyser's non-linear model, the system must be linearized around a point of operation in a permanent regime to apply linear control techniques. Working with incremental variables (ΔT_{el}, $\Delta \dot{T}_{el}$, ΔI_{el}, ΔT_{amb}, $\Delta \dot{Q}_{cool}$) around a chosen operating point, where:

$$\Delta \dot{T}_{el} = \dot{T}_{el} - \dot{T}_{el,0} = \dot{T}_{el}, \;\; \Delta T_{el} = T_{el} - T_{el,0}, \;\; \Delta I_{el} = I_{el} - I_{el,0},$$
$$\Delta T_{amb} = T_{amb} - T_{amb,0}, \;\; \text{and} \;\; \Delta \dot{Q}_{cool} = \dot{Q}_{cool} - \dot{Q}_{cool,0}.$$

Taylor series is applied to (5), and after calculating the partial derivatives, the following state-space equation is obtained:

$$\Delta \dot{T}_{el} = -a_c \Delta T_{el} + b_c \Delta \dot{Q}_{cool} + m_{1c} \Delta I_{el} + m_{2c} \Delta T_{amb}. \tag{6}$$

For better understanding, the variables in (6) are renamed as in (7):

$$\dot{x}(t) = -a_c x(t) + b_c u(t) + m_{1c} d_1(t) + m_{2c} d_2(t), \tag{7}$$

where $x(t)$ is the electrolyser temperature, $u(t)$ is the heat dissipated by cooling system, $d_1(t)$ is the electric current and $d_2(t)$ is the ambient temperature.

3. Proposed Control

Figure 1 shows the system that will be controlled and its input and output variables.

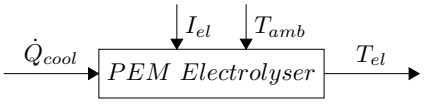

Figure 1: PEM electrolyser system.

The first step towards the proposed control is to determine the discrete model of the system. For this, the continuous model (7) was discretized using the zero-order hold (ZOH) mathematical model, where T_s is the sampling time:

$$\alpha = \frac{1 - e^{-a_c T s}}{a_c}, \;\; a_d = e^{-a_c T s}, \;\; b_d = \alpha b_c,$$
$$m_{1d} = \alpha m_{1c}, \;\; \text{and} \;\; m_{2d} = \alpha m_{2c}.$$

Resulting in (8):

$$x(k+1) = a_d x(k) + b_d u(k) + m_{1d} d_1(k) + m_{2d} d_2(k). \tag{8}$$

The proposed controller includes a CARIMA (Controlled Autoregressive Integrated Moving Average) model to incorporate a disturbance estimate and to give unbiased predictions in the steady state, irrespective of some parameter uncertainty.

The CARIMA model is expressed by (9), as presented by Camacho and Bordons (2007) to calculate the output predictions of the Generalized Predictive Controller:

$$a(z^{-1})y(k) = b(z^{-1})u(k) + \frac{c(z^{-1})}{\Delta}e(k), \tag{9}$$

where z^{-1} is the backward shift operator, the denominator of the perturbation model explicitly includes the integrator $\Delta = 1 - z^{-1}$, $e(k)$ is a white noise of zero mean, and the polynomial $c(z^{-1})$ will be a controller tuning parameter.

In this way, the disturbance model is included in (8), omitting the index d for simplicity, resulting in:

$$y(k) = \frac{b}{(1 - az^{-1})}u(k) + \frac{m_1}{(1 - az^{-1})}d_1(k)$$
$$+ \frac{m_2}{(1 - az^{-1})}d_2(k) + \frac{(1 + c_1 z^{-1} + c_2 z^{-2})}{\Delta(1 - az^{-1})}e(k).$$

The system output is divided into four parts corresponding to the four variables appearing in the previous equation, and predictions are calculated for each:

$$y(k) = y_1(k) + y_2(k) + y_3(k) + y_4(k). \tag{10}$$

Future outputs can be obtained using the state-space model through recursive calculations over an N-step prediction horizon. Predictions of $y_1(k)$:

$$\begin{aligned}
y_1(k+1|k) &= ay_1(k) + bu(k),\\
y_1(k+2|k) &= a^2y_1(k) + abu(k) + bu(k+1),\\
\vdots &\quad = \quad \vdots\\
y_1(k+N|k) &= a^Ny_1(k) + a^{N-1}bu(k) + \cdots + bu(k+N-1).
\end{aligned}$$

Predictions of $y_2(k)$:

$$\begin{aligned}
y_2(k+1|k) &= ay_2(k) + m_1d_1(k),\\
\vdots &\quad = \quad \vdots\\
y_2(k+N|k) &= a^Ny_2(k) + (a^{N-1}m_1 + \cdots + m_1)d_1(k).
\end{aligned}$$

Predictions of $y_3(k)$:

$$\begin{aligned}
y_3(k+1|k) &= ay_3(k) + m_2d_2(k),\\
\vdots &\quad = \quad \vdots\\
y_3(k+N|k) &= a^Ny_3(k) + (a^{N-1}m_2 + \cdots + m_2)d_2(k).
\end{aligned}$$

$y_4(k)$ is the disturbance model represented in the transfer function form. Equation (11) is used to transform it into state-space:

$$y_4(k) = \frac{c(z^{-1})}{\Delta(1-az^{-1})}e(k) = \frac{1 + c_1z^{-1} + c_2z^{-2}}{1 + \tilde{a}_1z^{-1} + \tilde{a}_2z^{-2}}e(k),$$

$$\begin{cases} x_4(k+1) &= Ax_4(k) + De(k),\\ y_4(k+1) &= Cx_4(k) + e(k). \end{cases} \tag{11}$$

The matrices of (11) are calculated from the observable-canonical form:

$$A = \begin{bmatrix} -\tilde{a}_1 & 1\\ -\tilde{a}_2 & 0 \end{bmatrix},\ D = \begin{bmatrix} c_1 - \tilde{a}_1\\ c_2 - \tilde{a}_2 \end{bmatrix},\ \text{and}\ C = \begin{bmatrix} 1 & 0 \end{bmatrix}.$$

Next, $e(k)$ is highlighted and replaced in (11), the equation of states $x_4(k+1)$:

$$\begin{aligned}
e(k) &= y_4(k) - Cx_4(k),\\
x_4(k+1) &= Ax_4(k) + D(y_4(k) - Cx_4(k)),\\
x_4(k+1) &= (A - DC)x_4(k) + Dy_4(k).
\end{aligned}$$

Prediction calculations for $y_4(k)$ are performed:

$$\begin{aligned}
y_4(k+1|k) &= CAx_4(k) + CDe(k),\\
y_4(k+2|k) &= CA^2x_4(k) + CADe(k),\\
\vdots &\quad = \quad \vdots\\
y_4(k+N|k) &= CA^Nx_4(k) + CA^{N-1}De(k).
\end{aligned}$$

Finally, the matrix of future outputs is determined in the function of the prediction matrices:

$$\begin{aligned}
y(k) &= Gu(k) + F_1y_1(k) + F_2y_2(k) + H_1d_1(k)\\
&+ F_3y_3(k) + H_2d_2(k) + F_4y_4(k) + Ee(k),
\end{aligned} \tag{12}$$

where,

$$G = \begin{bmatrix} b & 0 & \cdots & 0\\ ab & b & \cdots & 0\\ \vdots & \vdots & \ddots & \vdots\\ a^{N-1}b & a^{N-2}b & \cdots & b \end{bmatrix},\ U = \begin{bmatrix} u(k)\\ u(k+1)\\ \vdots\\ u(k+N-1) \end{bmatrix},$$

$$F_1 = F_2 = F_3 = \begin{bmatrix} a\\ a^2\\ \vdots\\ a^N \end{bmatrix},\ F_4 = \begin{bmatrix} CA\\ CA^2\\ \vdots\\ CA^N \end{bmatrix},\ E = \begin{bmatrix} CD\\ CAD\\ \vdots\\ CA^{N-1}D \end{bmatrix},$$

$$H_1 = \begin{bmatrix} m_1\\ am_1 + m_1\\ \vdots\\ a^{N-1}m_1 + \cdots + m_1 \end{bmatrix},\ \text{and}\ H_2 = \begin{bmatrix} m_2\\ am_2 + m_2\\ \vdots\\ a^{N-1}m_2 + \cdots + m_2 \end{bmatrix}.$$

Equation (12) is equivalent to, $Y = GU + f$, where f is the free response.

Equation (13) represents the cost function J. In MPC, it is essential to define the controller's objectives, select optimal control actions that minimise tracking errors, penalize unwanted variations in control signals, and ensure efficient and robust system performance:

$$J = (Y - W)^TQ(Y - W) + \Delta U^TR\Delta U + U^TSU, \tag{13}$$

in which Y is the future output matrix, W is the future trajectory reference matrix, ΔU is the control increments matrix, and U is the control effort matrix. Q, R, and S are diagonal weighting matrices that penalise tracking error, control effort, and the magnitude of the control action, respectively.

To simplify the calculations, ΔU is expressed as a function of U and u_0 as shown below:

$$\begin{bmatrix} \Delta u(k)\\ \Delta u(k+1)\\ \vdots\\ \Delta u(k+N-1) \end{bmatrix} = \begin{bmatrix} 1 & 0 & \cdots & 0 & 0\\ -1 & 1 & \cdots & 0 & 0\\ \vdots & \vdots & \ddots & \vdots & \vdots\\ 0 & 0 & \cdots & -1 & 1 \end{bmatrix} \begin{bmatrix} u(k)\\ u(k+1)\\ \vdots\\ u(k+N-1) \end{bmatrix}$$

$$- \begin{bmatrix} 1\\ 0\\ \vdots\\ 0 \end{bmatrix} u(k-1),\ \text{where}\ \Delta U = MU - Tu(k-1) = MU - u_0.$$

Replacing Y and ΔU in (13), we get:

$$\begin{aligned}
J &= (GU + f - W)^TQ(GU + f - W) +\\
&(MU - u_0)^TR(MU - u_0) + U^TSU.
\end{aligned} \tag{14}$$

Next, highlighting the role of U:

$$\begin{aligned}
J &= U^T(G^TQG + M^TRM + S)U +\\
&2((f - W)^TQG - u_0^TRM)U + \text{const.}
\end{aligned} \tag{15}$$

To calculate the optimal control, the minimum of J leads to:

$$U = (G^T QG + M^T RM + S)^{-1}(G^T Q(W - f) + M^T Ru_0). \quad (16)$$

In this way, the controller coefficients are calculated. K corresponds to the row matrix of the first portion of (16), k_e the second portion of (16), and k_r the sum of the elements of K:

$$K \rightarrow 1^{st} \text{ row of } (G^T QG + M^T RM + S)^{-1} G^T Q, \quad (17)$$
$$k_e \rightarrow 1^{st} \text{ row of } (G^T QG + M^T RM + S)^{-1} M^T RT. \quad (18)$$

Therefore, the control signal is as shown below:

$$u(k) = k_r r(k) - K(F_1 y_1(k) + F_2 y_2(k) + F_3 y_3(k) + H_1 d_1(k) + H_2 d_2(k) + F_4 y_4(k) + Ee(k)) + k_e e(k) + k_e u_0,$$

where,

$$\begin{aligned} F_4 y_4(k) + Ee(k) &= F_4 y_4(k) + E(y_4(k) + Cx_4(k)) \\ &= (F_4 - EC)x_4(k) + Ey_4(k), \\ k_e e(k) &= k_e(y_4(k) + Cx_4(k)) = k_e y_4(k) + k_e C x_4(k). \end{aligned}$$

Thus,

$$\begin{aligned} u(k) &= k_r r(k) - KF_1 y_1(k) - KF_2 y_2(k) - KF_3 y_3(k) \\ &- KH_1 d_1(k) - KH_2 d_2(k) - [K(F_4 - EC) + k_e C]x_4(k) \\ &- [KE - k_e]y_4(k) + k_e u_0. \end{aligned}$$

To simplify the expresion $u(k)$, F is adopted in place of F_1, F_2 and F_3, then:

$$u(k) = k_r r(k) - KF(y_1(k) + y_2(k) + y_3(k)) - KH_1 d_1(k) - KH_2 d_2(k) - [K(F_4 - EC) + k_e C]x_4(k) - [KE - k_e]y_4(k) + k_e u_0.$$

Renaming some coeficientes as,

$$K_1 = KH_1, \quad K_2 = KH_2, \quad K_3 = KF, \quad K_4 = KE - k_e,$$
$$K_5 = K(F_4 - EC) + k_e C, \quad V = K_5(zI - A + DC)^{-1}D + K_4,$$
$$\text{and } \hat{y}(k) = y_1(k) + y_2(k) + y_3(k).$$

Thus,

$$\begin{aligned} u(k) &= k_r r(k) - K_1 d_1(k) - K_2 d_2(k) - K_3 \hat{y}(k) - K_4 y_4(k) \\ &- K_5 x_4(k) + k_e u_0, \\ u(k) &= k_r r(k) - K_1 d_1(k) - K_2 d_2(k) - K_3 \hat{y}(k) - V y_4(k) + k_e u_0. \end{aligned}$$

The proposed control structure is depicted in Figure 2. The block $P(s)$ denotes the model of the PEM electrolyser process. The second saturation block incorporates the process saturation model, reflecting its physical constraints and ensuring the control signal remains within permissible limits. The first saturation block is essential to prevent the windup effect. For signal discretisation, the ZOH block is employed. Additionally, a continuous-to-discrete signal sampler is used post-process. Gains K_1, K_2, K_3, and k_e are designed to ensure system stability, while the robustness filter V enhances disturbance attenuation. The gain k_r ensures a unit static gain between the input and output, which is desired to follow constant references at a steady state.

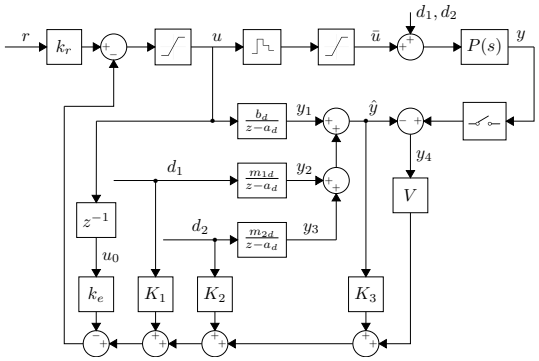

Figure 2: Proposed model-based predictor structure.

One of the main features of this controller is that, in the proposed configuration, it exhibits an action similar to a feedforward controller, allowing it to preemptively correct disturbances before they can significantly impact the process. Thus, it provides decoupling and additional freedom to the conventional MPC control. This advantage sets it apart from conventional control structures, delivering a superior output signal in terms of performance and robustness when measurable disturbances are present.

4. Simulation results

The proposed controller's design used a linearized model of a 1kW Hamilton-STD SPE-HG electrolyser from the Department of Systems Engineering and Automatic Control laboratory at the University of Seville. Some features of this system are $n_c = 6$ and thermal parameters $C_t = 9540J/K$ and $R_t = 0.11K/W$.

The simulations were conducted using MATLAB software (version R2023b) and the Simulink environment with a nonlinear model of the electrolyser. Measured data of electrical current supplied by photovoltaic (PV) generation and ambient temperature on a sunny summer day in Seville, Spain, collected on July 25, 2022, were used. The simulation time corresponds to 86400 seconds, equivalent to one measurement day (24h).

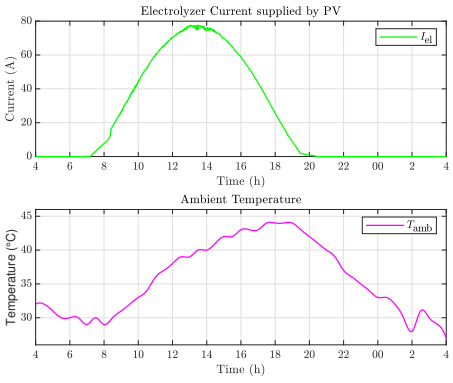

Figure 3: Disturbances (I_{el} and T_{amb}).

Figure 3 shows the two measurable disturbances of the system: I_{el}, current supplied to the electrolyser by the PV source, and T_{amb}, ambient temperature. The current applied

to the electrolyser is saturated at around 80 A since the allowable operating current range for this electrolyser is 5-80A, and this value could easily be exceeded under these climatic conditions.

The controller design begins by discretizing the linearized continuous model at an operating point ($T_{el,0}$ = 30ºC and $I_{el,0}$ = 40A) for a sampling time of 100 seconds.

$$\dot{x}(t) = -9.6832e^{-4}x(t) - 1.0482e^{-4}u(t) + 2.3090e^{-4}d_1(t) + 9.5293e^{-4}d_2(t),$$

$$x(k+1) = 0.9077x(k) - 0.01u(k) + 0.022d_1(k) + 0.0908d_2(k).$$

Choosing 40ºC as a reference, considering that temperatures slightly above this value would already contribute to the degradation of the PEM membrane, the proposed controller was adjusted to the following values: prediction horizon equal to 10, control horizon equal to 10, Q matrix weight equal to 1, R matrix weight equal to 0.5, S matrix weight equal to 0, c_1 and c_2 from the $c(z^{-1})$ polynomial are -1.62 and 0.6561, respectively.

As the cost function was calculated analytically without considering constraints, the weights Q, R, and S were defined based on a prior analysis or heuristic of performance requirements and system characteristics. Therefore, the primary objective was to minimise output errors (Q) and control increments (R) without directly penalising the magnitude of the control action ($S = 0$) since the added saturators, as shown in Figure 2, naturally impose limitations on control action.

The matrix R, which is related to the control increment, was adjusted so that $r(1,1) = 0$; in this way, the cost associated with the variation of the first control (Δu_1) will not be penalized in the control function cost. It modifies the cost function to allow more aggressive initial control action, providing more efficient setpoint tracking while maintaining the specified control and prediction horizons for the rest of the optimization process. However, this approach should be used cautiously to avoid potential oscillations or instability in the system.

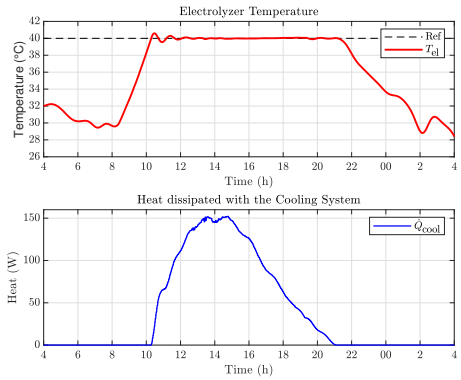

Figure 4: Output response (T_{el}) and control response ($\dot{Q}_{cool}$).

The proposed controller was applied to the electrolyser, generating Figure 4, in which it can be seen that the controller presents a good performance even though the process is nonlinear. The output signal exhibits little oscillatory behavior and soon reaches the desired reference value. At times when there is no current application and the ambient temperature value is lower than the desired reference, the electrolyzer output temperature will only be influenced by the ambient temperature, presenting similar behavior to it.

5. Conclusion

As highlighted in this paper, the temperature of the electrolyser is a crucial parameter to control, given its significant influence on performance and lifespan. Ensuring a desired reference, the proposed controller promises to increase efficiency in the electrolysis process, contributing to increased H_2 production and longer equipment life. The controller design uses model-based predictive control combined with a disturbance model to correct electrical current and ambient temperature variations before they significantly impact the electrolyser output temperature. It aims to maintain the temperature output signal at a desired value with good performance and robustness in the face of non-linear variations in disturbances applied to the process. The proposed strategy's calculations were conducted analytically, but future work will implement an optimization algorithm to achieve optimal control, proposing a comparison between the two types of controllers.

Acknowledgement

Financial support from the Brazilian funding agency CAPES (Brazil) [Grant Numbers 88887.636100/2021-00, 88881.892669/2023-01] and CNPq (Brazil) [Grant Numbers 313000/2021-2, 422633/2021-6, 421770/2023-6, 312512/2022-8], and from the grant PID2022-142069OB-I00 funded by MCIN/AEI/10.13039/501100011033/FEDER, UE is gratefully acknowledged.

References

Benghanem, M., Almohamadi, H., Haddad, S., Mellit, A., Chettibi, N., 2024. The effect of voltage and electrode types on hydrogen production powered by photovoltaic system using alkaline and pem electrolyzers. International Journal of Hydrogen Energy 57, 625–636.

Camacho, E., Bordons, C., 2007. Model Predictive control. Advanced Textbooks in Control and Signal Processing. Springer, London.

Carmo, M., Fritz, D. L., Mergel, J., Stolten, D., 2013. A comprehensive review on pem water electrolysis. International Journal of Hydrogen Energy 38, 4901–4934.

Espinosa-Lopez, M., Darras, C., Poggi, P., Glises, R., Baucour, P., Rakotondrainibe, A., Besse, S., Serre-Combe, P., 2018. Modelling and experimental validation of a 46 kw pem high pressure water electrolyzer. Renewable Energy 119, 160–173.

Keller, R., Rauls, E., Hehemann, M., Müller, M., Carmo, M., 2022. An adaptive model-based feedforward temperature control of a 100 kw pem electrolyzer. Control Engineering Practice 120, 104992.

Maia, R. G. T., Garcia, K. C., 2023. What they say, what they do and how they do it: An evaluation of the energy transition and ghg emissions of electricity companies. Energy Policy 174, 113462.

Molina, P., Rios, C., de Leon, C. M., Brey, J., 2024. Heat management system design and implementation in a pem water electrolyser. International Journal of Hydrogen Energy.

Mora, M., Bordons, C., 2022. Desarrollo y validación experimental del modelo dinámico de un electrolizador pem de 1kw para su integración con generación renovable. XLIII Jornadas de Automática: libro de actas, 560–567.

Ogumerem, G. S., Pistikopoulos, E. N., 2020. Parametric optimization and control for a smart proton exchange membrane water electrolysis (pemwe) system. Journal of Process Control 91, 37–49.

United Nations, 2015. The 2030 agenda for sustainable development. https://sustainabledevelopment.un.org/post2015/transformingourworld, accessed: 2024-05-28.